Real-time sub-Ångstrom imaging of reversible and irreversible conformations in rhodium catalysts and graphene

Christian Kisielowski, Lin-Wang Wang, Petra Specht, Hector A. Calderon, Bastian Barton, Bin Jiang, Joo H. Kang, and Robert Cieslinski

Phys. Rev. B **88**, 024305 — Published 29 July 2013

DOI: 10.1103/PhysRevB.88.024305

Real-Time, Sub-Ångstrom Imaging of Reversible and Irreversible Conformations in Rhodium Catalysts and Graphene

Christian Kisielowski[+*], Lin-Wang Wang[++], Petra Specht[+++], Hector A. Calderon[#], Bastian Barton[##], Bin Jiang[###], Joo H. Kang[†], Robert Cieslinski[†]

[+] National Center for Electron Microscopy and Joint Center for Artificial Photosynthesis, Lawrence Berkeley National Laboratory, One Cyclotron Rd., Berkeley CA 94720 / USA

[++] Material Sciences Division, Lawrence Berkeley National Laboratory, One Cyclotron Rd., Berkeley CA 94720 / USA

[+++] Department of Material Science & Engineering, UC Berkeley CA 94720 / USA

[#] Dept. Fisica, ESFM-IPN, Mexico D.F. 07300, Mexico

[##] FEI Company, Eindhoven, The Netherlands

[###] FEI Company, 5350 NE Dawson Creek Drive Hillsboro, Oregon 97124, USA

[†] The DOW Chemical Company, Midland MI 48667 / USA

PACS: 34.80.Dp, 61.48.Gh, 68.37-d, 81.16.Hc, 82.37.Gk

Corresponding Author

* CFKisielowski@lbl.gov

ABSTRACT

The dynamic responses of a rhodium catalyst and a graphene sheet are investigated upon random excitation with 80 kV electrons. An extraordinary electron microscope stability and resolution allow studying temporary atom displacements from their equilibrium lattice sites into metastable sites across projected distances as short as 60 pm. In the rhodium catalyst, directed and reversible atom displacements emerge from excitations into metastable interstitial sites and surface states that can be explained by single atom trajectories. Calculated energy barriers of 0.13 eV and 1.05 eV allow capturing single atom trapping events at video rates that are stabilized by the Rh [110] surface corrugation. Molecular Dynamics simulations reveal that randomly delivered electrons can also reversibly enhance the sp^3 and the sp^1 characters of the sp^2-bonded carbon atoms in graphene. The underlying collective atom motion can dynamically stabilize characteristic atom displacements that are unpredictable by single atom trajectories. We detect three specific displacements and use two of them to propose a path for the irreversible phase transformation of a graphene nanoribbon into carbyne. Collectively stabilized atom displacements greatly exceed the thermal vibration amplitudes described by Debye-Waller factors and their measured dose rate dependence is attributed to tunable phonon contributions to the internal energy of the systems. Our experiments suggest operating electron microscopes with beam currents as small as zepto-Amperes / nm^2 in a "weak-excitation" approach to improve on sample integrity and allow for time-resolved studies of conformational object changes that probe for functional behavior of catalytic surfaces or molecules.

Introduction

In the recent past significant initiatives have been dedicated to the exploration of sustainable energy solutions[1-6]. Certainly, related research must address a rich diversity of challenges because it is not only the static arrangement of matter that must be understood at a single atom level but also its collective behavior that leads to functionality. Moreover, hybrid materials are now commonly explored to enable more complex functions. Traditionally, electron microscopy is considered the method of choice to unravel the static structure of materials at atomic resolution. This view is further strengthened by recent technological advancements, which enable atomic resolution at elevated temperature and pressure[7-10], dynamic electron microscopy with a time resolution of picoseconds or even femtoseconds[11, 12] at 0.3 - 0.4 nm of spatial resolution[12] and aberration-corrected electron microscopy with deep sub-Ångstrom resolution and single atom sensitivity[13-16]. Such exceptional progress has nourished a growing expectation to provide equipment and concepts, which will enable capturing the dynamic behavior of matter with single atom sensitivity at atomic resolution in thermodynamically relevant conditions.

However, significant uncertainties must be addressed before the emerging visions can be forged into feasible experiments. In this respect it is urgent to address the view that electrons of mid-voltage energies around 300 keV and lower necessarily damage hybrid materials too much to maintain structural integrity at atomic resolution. In this energy range, there is a rapid displacement of atoms that are bonded to corners, edges and surfaces of nanocrystals or catalysts since the binding energies to these sites are lowered compared to bulk values[17,18]. In addition, ionization damage is known to be most hazardous to the soft matter components [19-21] of hybrid materials. Noteworthy, it is unsettled to date to what extend electron beam-induced structure

alterations are reversible or irreversible [22]. In the presence of strong beam-sample interactions the achievable resolution is commonly described by[23]:

$$d = (d_i^{\,2} + (S/N)^2 / (C^2 * D))^{1/2} \qquad (1)$$

Equation 1 relates the achievable resolution d to the image contrast C, the signal to noise ratio S/N, the accumulated electron dose D, and the native point resolution of the instrument d_i. In biological specimens D cannot exceed ~ 1000 e/nm^2, which only allows resolving a few Ångstrom and prohibits single atom sensitivity[19]. By comparison, the atomic resolution imaging of a single carbon atom in graphene sheets with a fair S/N ratio typically requires a sample exposure to 10^6 electrons / nm^2, which greatly exceeds threshold values for molecules. Therefore, atomic resolution imaging of molecules, small atom clusters or surface structures remains a Grand Challenge in basic sciences [24].

Consequently, new concepts are developed and tested that address atomic resolution imaging of radiation sensitive materials. A most successful approach pursues strong object excitations with x-rays from a pulsed, free electron laser[25]. The method builds on capturing diffraction patterns within femtoseconds after excitation to outrun the unavoidable material decomposition (Figure 1, top). Alternatively, it is proposed to determine the three-dimensional conformations of macromolecular assemblies at atomic resolution from large data sets of images each recorded with ultra-low-signal, S/N << 3 (Figure 1, bottom)[26, 27] even beyond current practices in biological sciences. Implicitly, any such "weak excitation" method assumes that object excitations into higher energy states are reversible and not accompanied by uncontrolled atom loss as symbolized at the top of Figure 1. If such models apply, one would expect that dose rates

dD/dt should become more important than the accumulated electron dose D in equation (1) and one could expect maintaining structural integrity at a larger accumulated electron dose if it is delivered at a small dose rate. Recent experiments with rhodium catalysts point to this direction[28].

This paper reports on previously uncontrolled phonon excitations that often dominate beam-sample interactions if atomic resolution imaging is practiced. It will be shown that such excitations can be tuned by electron dose rates to intentionally stimulate reversible or irreversible structure alterations. The finding opens room for the deployment of a weak-excitation approach for electron microscopy that also allows exploring the gray zone between both extremes of Figure 1. It is enabled by a recently developed in-line holography concept with dose rate variations by orders of magnitude at acceleration voltages between 20 kV and 300 kV[29]. The currently obtainable time resolution is in the range of minutes to milliseconds and one can address turn-over-frequencies of chemical reactions for example. We demonstrate the validity of the concept by detecting phonon assisted single atom trajectories and atom displacements by phonon excitations that create structure alterations relevant to the onset of functional system behavior.

2. Results

2.1 Experimental details

Our experiments are performed with the TEAM 0.5 microscope operated at 80 kV. Details of its capabilities are published elsewhere [13, 29]. In brief, we achieve deep sub-Ångstrom resolution

and long time stability[30] by protecting an aberration-corrected status of the microscope with the voltage-dependent [29] and small chromatic-aberration coefficient C_c of an Ultra-Twin objective lens[31] and by narrowing the energy spread of the high-brightness Schottky field emitter with a monochromator[32]. Residual lens aberrations are removed post image acquisition during numerical reconstruction of the electron exit wave functions that creates the in-line holograms[33]. In this process, the recorded focus series of images are aligned to a precision of 2.4 pm[34]. The instrument is tuned to a negative spherical aberration coefficient C_s = - 15 µm and structural images of thin samples occur at an overfocus of ~ 10 nm[35]. In this configuration TEAM 0.5 exhibits an extraordinary small focus drift Δf_d of only 0.4 nm during minutes of recording time[29], which is significantly smaller than the resolution limiting focus spread Δf_r of 0.7 nm[33]. The deep sub-Ångstrom resolution between 0.06 - 0.07 nm of the microscope at 80 kV is shown in Figure 2 by resolving an adequate dumbbell spacing in GaN [112].

Since $\Delta f_d < \Delta f_r$ the acquired images are limited by resolution and not by drifting aberration coefficients[30]. This condition must be fulfilled to reliably interpret contrast changes across distances as small as 0.06 nm to 0.1 nm in experiments that last minutes. Further, we bypass the traditional condenser system using a new monochromator assisted illumination scheme[28] and only expose sample areas of 400 - 900 nm^2 that are matched to the size of the CCD camera at high resolution. Thereby, we eliminate any unnecessary sample exposure to the electron beam, which causes uncontrolled damage. In the past, attempts to approximate this situation were mostly sacrificed to accommodate a larger field of view. Moreover, the new illumination scheme allows for rapid dose rate adjustments by orders of magnitude[28]. Exposure times vary between 0.1 and 1 second and the images are recorded with a sampling rate of 0.02 - 0.03 nm / pixel. For a detailed image analysis they are re-sampled on a grid of 6 pm pixel size using a bilinear

extrapolation scheme, which is possible without increasing noise because of the high signal to noise ratio of better than 10:1 from 1 carbon atom in a reconstructed wave function. Our re-sampling process did not reach beyond 1/8 of a pixel size because smaller values approach the precision as to which images are aligned in the reconstruction process of the exit wave function. Other image processing routines include the extraction of an averaged motive and its standard deviation by cross-correlation averaging, which is a procedure that is commonly employed to boost the S/N ratios from identical objects in biological samples[36] and a solution to the phase problem by reconstruction of the complex electron exit wave function from focus series of real space images[29]. The MacTempas software package[37] is used to apply these procedures. In addition, the software allows for image simulation by multislice calculations using theoretically predicted atom positions as input parameters.

Density functional theory (DFT) under the generalized gradient approximation (GGA)[38] is applied to calculate the graphene and rhodium systems. Projector augmented-wave pseudopotentials[39] are used as implemented in the VASP code[40]. Transition path potential barriers are calculated by the nudged elastic band method (NEB)[41] for a rhodium thin film slab that containes 144 atoms arranged in 2 monolayers. The behavior of interstitial atoms is calculated for the face centered cubic (fcc) structure of rhodium using a periodic supercell containing 108 rhodium atoms arranged in 3x3x3 fcc cubes with a 3x3x3 Monkhorst-Pack k-point set for the supercell. The periodic supercell for graphene contains 24 atoms and is used with 5x5x1 Monkhorst-Pack k-points. Ab-initio Molecular Dynamics (MD) simulations are carried out at average temperatures of 2500K, 5000K, 7500K and 10000K with time intervals of 2 femtoseconds. C-C bonds are constantly breaking and reforming at 10000 K and the graphene structure is lost. Therefore, we used 10000K as an approximated melting point temperature T_m of

graphene. Experimentally, the solid/liquid phase transition temperature of graphite is ~ 4000 K[42] but it is known that the melting point of a graphene sheet is significantly higher because of absent interlayer carbon bonds.

Rhodium catalysts were prepared by impregnation of alumina with an aqueous solution of rhodium chloride and ammonium metatungstate to yield 2 wt % rhodium and rhodium to tungsten ratio to be 1. The impregnated catalyst was reduced in hydrogen at 300 ºC and dispersed on holey carbon grids for observation. In the context of this paper, the catalysts are treated as rhodium crystals and expectable contributions from the tungsten co-deposition will be reported elsewhere. The fabrication of exfoliated graphene sheets for imaging with electron beams has been reported and includes a prolonged exposure of single graphene layers to the high energetic electron beam. This removes all unwanted surface contaminants on a time scale of half an hour and eventually creates holes in exposed sample areas[43]. Finally, the strontium titanate (STO) samples are prepared in cross-section geometry by mechanical polishing, ion beam processing and thermal treatment. All measurements were done at room temperature.

2.2 Reversible atom displacements in a rhodium catalyst.

Our investigation builds on previous reports about electron beam-induced atom displacements in thin films [22, 44, 45] that are sample thickness dependent[46] and most prominent in surface proximity and in nanocrystals consisting of a few atomic layers. A sequence of images from the central part of a rhodium catalyst is shown in Figure 3 at a magnification that allows observing sub-Ångstrom atom displacements by visual inspection. Atom columns appear bright on a dark background and contain 2-3 atoms on an average (thickness: ~ 0.6 nm)[22]. Since the phase

contrast from atoms in thin films increases with their atomic number $Z^{2/3}$ (Z_C=6, Z_{Rh}=45, Z_W=74)[47] the rhodium contrast is strong and should be constant. Instead, it greatly fluctuates during observation as reported earlier[22]. There, the contrast fluctuations have been attributed to electron beam-induced phonon excitations resulting in 3D low frequency atom displacements, which are assumed to be random. A better impression of the seemingly continuous contrast fluctuations in image series is provided by the supplementary movie-Rh. Expending our previous work, Figure 3 points out that such temporary generated contrast appears systematically close to the projected tetragonal interstitial sites that are marked by I_T in Figure 4a. These sites are separated by a projected distance of only 95 pm from lattice site positions. Their three-dimensional separation distance is 0.165 nm. Moreover, any contrast that is generated in the space between lattice sites also disappears in a successive frame of Figure 3. Rarely, we detect similar contrast variations occurring close to the octahedral interstitial sites I_O (Figure 4a), which suggests that they are not random but site specific. Equally important, the experiment documents that the crystal structure and its occupation with Rh atoms is maintained throughout the observation time. This requires that all underlying excitations are entirely reversible in suitably chosen current and voltage conditions. Thus, the randomly delivered electrons do not cause random excitations, only. Instead, they thermalize into distinct metastable structures that can be observed as time dependent deviations from an average structure and modeled as shown next.

First we consider rhodium atoms that are displaced from their lattice site into interstitial sites and create Frenkel pairs. Such displacements are unstable if they occur into a nearest tetrahedral interstitial site because the generated interstitial / vacancy pair will recombine as indicated from our DFT calculation. In contrast, an atom displacement into a second nearest tetrahedral site or the nearest octahedral site creates a metastable situation of prolonged lifetime. In the experiment

we rarely observe contrast formation in octahedral interstitial sites and one must speculate about reasons why displacements into the second nearest tetrahedral interstitial sites are preferred. However, a most stunning agreement between the calculation and the experiment is achieved by considering atom trapping into surface states of the 0.6 nm thin crystal. Results of these calculations are shown in Figure 4b where the characteristic displacement trajectory of an excited Rh atom is described by steps 0 through 5 and inserted into the experimental image. The excellent match of its path to the generated extra contrast between atom columns allows us to identify this event as one origin for the temporary contrast generation. Figure 4c depicts total energy GGA calculations for this displacement including the activation of a rhodium atom across an energy barrier of 1.05 eV for the excitation process and of 0.13 eV for recombination. Since total energy calculations typically underestimate barrier heights, we expect the actual barrier might be larger. These energies can be compared to binding energies between 1.7 and 4.6 eV for rhodium atoms in small clusters that decreases with decreasing crystal size[48]. Obviously, the internal energy of atoms bound in small clusters or to surfaces can be raised by electron irradiation to reach stability limits. Finally, the inserted view of the Rh crystal in Figure 4c shows that the excited atom is temporarily captured in the channel of the corrugated [110] surface.

2.3 Reversible atom displacements in graphene.

Having established a reasonable explanation for the contrast fluctuations, a deeper understanding of basic principles benefits from a simpler sample structure, which is why we resorted to investigating graphene, a single layer of sp^2 bonded carbon atoms. The signature of temporary carbon atom displacements is even weaker in graphene than in rhodium because of the

reduced scattering power of the light element. In essence, we aim now at the detection of a fractional contrast from a single carbon atom that may be as weak as the phase contrast signature from a single hydrogen atom. Therefore, we reduce noise by recording focal series of 20 images from graphene that are reconstructed to obtain the complex electron exit wave function with an enhanced S/N ratio [29, 31].

A resulting phase image of graphene is shown in Figure 5a. It depicts its time-averaged structure at atomic resolution with a signal to noise ratio that cannot be matched by another method using an equal electron dose at the given magnification. Again, we display the image at a large magnification to allow for an identification of irregularities by visual inspection: Two most recognizable events A and B are pointed out by arrows and a horizontal line eases the recognition of vertical atom displacements that reach tenth' of picometers. The magnitude of the existing atom displacements from their equilibrium positions is determined by repetitively measuring the projected 0.14 nm C-C dumbbell distances across the entire image of Figure 5a using a refined peak fitting procedure. This method has been previously established and applied to extract the equivalent 0.14 nm Ga-As dumbbell distance in a 7 nm thick GaAs sample[34]. Both measurements are compared in Figure 5b and it is seen that the data spread $2\sigma = 46$ pm in graphene exceeds the equivalent GaAs value by a factor of 10. Next, we amplify contrast from additional but weaker site specific displacements events in Figure 5a by cross-correlating the hexagonal atom structure of graphene to every equivalent cell in the image, which allows calculating an average motive with improved S/N ratio and its standard deviation. The results are shown in Figures 5c and 5d, respectively. Of specific interest is the standard deviation image since it does not exhibit random noise but a modulated intensity pattern with accumulated contrast in positions A, B, and C. They are distinguishably different from the nearby lattice sites

because of the sub-Ångstrom resolution of the instrument. In graphene, however, both the large atom displacements from Figure 5b and the accumulation of additional contrast in specific locations in Figure 5d cannot be understood by modeling single atom trajectories since activation barriers for excitations are large and recombination is immediate.

We test the hypothesis that metastable states or Eigenmodes can emerge from collective system excitations. Indeed, our MD simulations that are summarized in Figure 6, Figure 7 and in Table 1 strongly support this view. The Figure 6a shows histograms of calculated atom displacements that are extracted from 24000 configurations of graphene and by a projection of the 3-dimensional atom displacements into an image plane. We consider four different temperatures between the melting point and a quarter of the melting point temperature. It is seen that the most common displacements u at the maximum of the distributions shift towards larger values with increasing temperature from 11 pm to 18 pm (Table 1). If one attributes u to a Debye-Waller factor $B = 8\pi^2u^2$, values between 1 and 3 $Å^2$ are calculated (Table 1) that agree well with experimentally determined bulk values of graphites between 1 - 2 $Å^2$ at room temperature[49]. Most remarkable, however, is the pronounced skewness of the distribution that increases with temperature because of a rapidly increasing number of displacements larger than 30 pm, that certainly exceed reasonable values for Debye-Waller factors (Figure 6b). Table 1 lists the number of displacements larger than 30 pm as a fraction of the total displacements. Such a ratio increases to 23% at 0.75 T_m. The spatial distribution of all atoms with respect to a central carbon atom and its next neighbors is shown in Figure 6c and Figure 6d for 0.5 T_m and 0.75 T_m. A comparison of both Figures highlights a dominantly random data distribution at low temperature. However, site-specific excitations emerge from this distribution into positions A and B as the temperature increases. At a temperature of ~ 0.75 T_m about a quarter of all

displacements exceed 30 pm, which makes large atom displacement a most common event and detectable in micrographs with deep sub-Ångstrom resolution. Therefore, we conclude that random phonon excitations of the entire object can temporary stabilize site-specific atom displacements, which we observe in the micrographs. Since such displacements are site specific (systematic) they do not vanish upon averaging. More generally, the question how structure emerges in objects upon random excitations has sparked debates about entropy since the early developments of thermodynamic concepts[50].

The Figure 7 provides a better understanding of the phenomenon and its relation to the experiment. Two snapshots of the MD simulations are shown in top and side views. They both present significant deformations that the simulated graphene sheet experiences upon thermal excitation (Figures 7a, 7b). Out-of-plane displacements occur with amplitudes as large as 0.15 nm. Thus, the sp^2 bond character of carbon atoms in graphene is locally altered to include sp^1 and sp^3 bonding components that create chain-like structures and tetrahedral configurations locally. Fleeing ring structures are formed from 5 and 7 carbon atoms. The difference between random and directed displacements in images from graphene is shown in Figure 7c by multisclice simulations. We assume a Debye-Waller factor B = 1 $Å^2$ to describe random displacements and utilize the calculated atom coordinates from the MD simulations to describe all directed displacements that occurred over a time period of 100 femtoseconds. The differences in such images (and in the corresponding phase images of a simulated electron exit wave function) are significant since directed structural changes cause contrast fluctuations and displacements far beyond values that one may expect from Debye-Waller factors. In particular, preferential displacements can be identified that include the sites A and B in this example, which are measured in the experiment as shown by the inset in Figure 5a. Therefore, we conclude that

collective atom excitations can temporary stabilize large atom displacements that occur irregularly in time as a result of a suitable displacement of many atoms and long-range interactions. One may call them "rare events". In fact, it was reported earlier[51] that the integration of long-range interactions into calculated phonon dispersions in graphite explains modes that include a translation of carbon atoms from their lattice site towards locations B and C, as observed in our experimental image in Figure 5d. In more general terms we observe the channeling of random phonon excitations into a few site-specific displacements that point towards possible structural evolutions. It is tempting to apply this knowledge and predict a transformation path for the phase transformation of graphene into carbyne.

2.4 Irreversible phase transformation of grahene into carbyne

A graphene sheet is transformed into linear chains of sp^1-bonded carbon atoms by electron irradiation as described in literature[52,53]. The movie-C in the supplementary information depicts the entire process. Four snapshots of this phase transformation are displayed in Figure 8a: In frame # 1 two adjacent holes are created by irradiation with a dose rate of $5\ 10^6$ e/nm^2/sec, which remain separated by a narrow graphene bridge. The bridge width is further reduced by preferentially removing carbon atoms from edge positions[43] until structure fluctuations occur in frame # 25 and carbon chains form spontaneously that are ~1 nm long.

Surprisingly, the carbon chains remain stable during the extreme electron illumination and 13 successive images are acquired (#27 - #39, accumulated dose: $9\ 10^7$ e/nm^2) before the chains disintegrate in frame # 40. Significant chain displacements occur during their observation, which are most obvious in the supplementary movie-C, but interchain cross-linking is not observed. In

spite of their motion, atomic resolution is achieved in frame # 31 and shown in Figure 8b. In frame #34 a kink was formed with an angle of $(116\pm8)^0$ (Fig. 8c). Topologically, the temporary formation of this kink from a previously straight line requirs a chain length extension from 1.0 nm (includes 9 carbon atoms) to 1.2 nm that must be accommodated by the addition of at least one extra carbon atom to the chain length if the average bond distance of 0.13 nm is to be preserved.

Short chains of carbon atoms are known as carbynes[54] and they form polytypes with alternating single and triple bonds (polyyne) or double bonds (cumulene) as shown in Figure 8c [55]. Kinks form on both polytypes with characteristic angles $\alpha = 115 - 120^0$ for polyyne and $\alpha' = 155 - 158^0$ for cumulene[55]. Therefore, a measured kink angle of $(116\pm8)^0$ reveals that polyyne is formed in our experiments in agreement with the theoretical expectation that polyynes are more stable than cumulenes[56]. However, the beam-induced chain displacements also suggest that bond alterations between single, double and triple bonds must occur just as in the case of graphene where hybridization is affected. Therefore, structure fluctuation between polyyne and cumulene can occur but they are undetectable by bond length measurements within the experimental error of Figure 8b. Most remarkable is the fact that the chains do not disintegrate immediately in the high energetic electron beam but maintain conformations over extended time periods. Carbon atoms can even be added or removed from the chains. This unexpected behavior can be understood if one accepts that bonds break rapidly during the observation but reform faster than atoms can be removed. This process can be called "self-healing".

Since possible phase transformation trajectories from graphene into carbyne are unknown, we use now the measured excitations of carbon atoms in graphene into the locations B and C from Figure 5d as a guideline to produce the geometrical transformation model shown in Figure 8d.

The process is irreversible because it is accompanied by 33% atom loss. The detailed match of the resulting geometrical model with the experiment in Figure 8e supports the interpretation that collective excitations direct the displacement of carbon atoms in the graphene bridge and stimulate this irreversible phase transition. Modeling single atom trajectories cannot capture this mechanism.

2.5 Dose rate dependences

Since the observed atom displacements are electron beam-induced, one must observe a contrast reduction in high-resolution images with an increasing dose rate (beam current). This contrast behavior becomes only observable after minimizing experimental artifacts related to the CCD camera or to sample drift. It must occur from a physical point of view because an increasing number of impinging electrons will rapidly increase local phonon emissions that successively displace atoms from their equilibrium position and soften the electron scattering potential. For this reason we acquire focal series of images with varying dose rates from the rhodium crystal and a STO confirmation sample. The figure 9a shows that contrast decreases logarithmically with the dose rate in both cases. In rhodium it decreases by a factor of larger than 2 if the beam current increases from 4 10^3 e/nm^2/s to 6 10^5 e/nm^2/s. Contrast losses by 50% or more are known as unexplainable mismatches between experimental images and image simulations[28]. Here we find, they are caused by beam-induced phonon excitations. From the magnitude of the effect one concludes that dynamic contributions to the image formation process can even exceed electron scattering contributions from static objects in conditions for traditional high-resolution imaging. In view of this significant contrast loss, imaging in low dose rate

conditions is greatly beneficial. In addition, there is significant room to study the dynamic behavior of matter by interpreting the dose rate dependence of contrasts as demonstrated in this paper.

Alternatively one may quote molecule motion across surfaces as a possible cause for a fluctuating contrast. However, the contrast change with dose rate (0.5 rad measured compared to ~ 0.1 radian for the contrast of light atoms or molecules) and the reproducibility of the effect (data set Rh: S1 = S4 or data set STO: S2=S3) that are shown in Figure 9a exclude such interpretations.

In our image simulations we distinguish between thermal excitations and dose rate effects using ordinary Debye-Waller factors of bulk materials and describing the beam-induced atom displacements by a Gaussian damping function with dose rate dependent vibration amplitudes. In the past, the procedure was used to accommodate mechanical microscope instabilities[57] that largely exceed the displacements, which we consider here. It is shown in Figure 9b that damping amplitudes between 68 pm and 40 pm accurately describe the phase signal enhancement in Figure 9a that is caused by decreasing dose rates from 6 10^5 e/nm^2/s to 4 10^3 e/nm^2/s. From the MD simulations of Figure 6 one estimates that the difference of ~30 pm corresponds to a temperature reduction of ~ 0.25 Tm in the simulation. It is also seen that all lateral atom displacements smaller than the assumed damping amplitude are undetectable except for their contribution to a reduction of the average signal strength. Only if lateral displacements occur greater than the average damping amplitude and only if they exhibit a lifetime that is comparable to the image exposure time, they can be captured in an image. In this sense, the finite image exposure time acts as a filter that enhances the detection of lateral structure alterations that present the *successful* attempts of the excited system to alter its structure.

3. Discussion and Conclusions

Egerton et al. recently reviewed beam-sample interactions[20]. Beyond their considerations, Jiang and Spence[58] suggested a spontaneous structure restoration as a possible mechanism for restoring materials integrity upon sample excitation above threshold values. This aspect of "self-healing" is explored here by dose-rate-controlled aberration-corrected electron microscopy.

The Figure 10a shows the available parameter space for such experiments in the TEAM 0.5 microscope by depicting the power P = U*I, which is generated by a beam current I of electrons that are accelerated by a voltage U. Scaled to square meters, the available power can exceed 10^{12} Watts/m^2. Obviously, any small, absorbed fraction of this available power would vaporize any solid. However, the maximum power can easily be reduced by 9 orders of magnitude upon current reduction, only. Atomic resolution imaging with atto-Amperes or less, however, would hardly create contrast above noise with typical image exposure times of 1 second. Therefore, we employ in-line holography to create a single image from hundreds of frames that are recorded over several minutes[29]. Acceleration voltages can be altered between 20 kV and 300 kV while maintaining atomic resolution[29]. Compared to current variations, such voltage differences change the power deposition marginally. Nonetheless, beam-sample interactions are most commonly discussed in the context of voltage dependent ionization or displacement damage[20], which are certainly relevant processes that, however, are rarely distinguished from beam-induced phonon excitations. The present phonon excitations are well documented in early work[59] and in recent time resolved measurements[12]. Such time resolved measurements also suggest that we do not observe short time excitations in the electronic structure of the materials but atomic motions in

the thermalization process. In this regime the lifetime of phonons approaches the average delivery time for electrons, which is set by dose rates. As a result, we expect observing dose rate dependent contrast modulations. The relevance of reversible excitations becomes very obvious if one estimates the energy E per volume V, which is dissipated in the sample and by[60]:

$$E/V = n*\rho*dE/dx \qquad (2)$$

Here, n is the accumulated number of impinging electrons per unit area, ρ is the material density, and dE/dx is the stopping power e.g. the energy dissipated per unit mass-thickness. This estimate is shown in Figure 10b where we used ρ= 3.5 g/cm^3, dE/dx =3*10^6 eVcm^2/g (at 60 kV) and 177 carbon atoms/nm^3 for the specific case of the cubic diamond structure. We consider the accumulated electron dose, only, which obviously omits any rate dependences. For a light element as carbon, two third of all scattering events are inelastic. Moreover, the energy densities are compared with formation energies of selected molecules and with total energies of small nanocrystals that may contain 1000 atoms or so. It is seen that an accumulated dose of only 1000 electrons/nm^2 already increases the inner energy per carbon atom by several eV, which already exceeds the formation energy of water molecules during observation. Therefore, it seemed reasonable to accept such low dose values as an upper boundary for damage-free imaging of soft matter as practiced for biological samples. In atomic resolution imaging, an accumulated dose of typically 10^5 – 10^6 electrons/nm^2 is used that most certainly exceeds any reasonable binding energy of single atoms. Even if this energy is shared between ~ 1000 atoms an excitation of a few eV/atom would remain, which is enough to cause sample decomposition or melting. In light of this estimate, it should be entirely impossible to image a single chain of 10 carbon atoms with

an accumulated dose of 10^8 e/nm^2 (Figure 8) without acknowledging the existence of reversible excitations and a concept of self-repair.

It is of interest considering how the available energy is stored in the object. Unlike a conventional illumination system in a TEM, we match the illuminated sample area to the field of view defined by the CCD camera, which allows us controlling the number of scattering events in the sample and enables tuning the inner energy of the system. Using a beam current of 10^5-10^6 e/nm^2/s and a 30 nm x 30 nm large field of view, 10^8 - 10^9 high energetic, inelastic scattering events occur in each second if every electron participates. Most obvious contributions to the internal energy U of an elastic medium include:

$$U = T S + \tfrac{1}{2} \sigma_{ij} \varepsilon_{ij} \qquad (3)$$

Here, T is temperature, S is entropy, and $1/2\ \sigma_{ij}\varepsilon_{ij}$ is the elastic energy described by general expressions for stress and strain, respectively. It is beyond the scope of the paper to quantitatively untangle all contributions from beam-sample interactions to the internal energy of the investigated samples at this point in time. Instead, it is noted that time resolved TEM experiments with graphite currently emerge that aim at performing this task with femtoseconds of time resolution and a spatial resolution of a few Ångstrom[12]. Concerning the structural dynamics of graphite[61] or graphene a converging view emerges that Debye-Waller factors alone cannot explain the measured mean-square atom displacements in excited samples. Instead, their explanation requires a strong coupling of phonons and many particle interactions.

In our simulations the increase of internal energy is entirely attributed to temperature, which would increase by hundreds of degrees in high dose rate conditions unless temperature is rapidly

channeled into the substrate that holds the investigated samples in place. Alternatively, entropy would moderate any temperature increase since it contributes to the specific heat of materials through the logarithm of a partition function. An expected logarithmic contribution of the numerous beam-induced object vibrations to the internal energy of samples is consistent with the observed logarithmic dependence of image contrast on dose rates. Both aspects are quite relevant since dynamic measurements of a phase transition in Cu_2S nanocrystals recently verified that a sample irradiation with a high dose rate increases temperature by only a few degrees[62] and it is known that electron beam-induced temperature increases can be small[63]. Elastic contributions to the internal energy would increase quadratic with increasing atom displacements and appear most prominent in small nanocrystals, thin films and in surface proximity, were binding energies are lowered and materials are more flexible. Again, this expectation is in excellent agreement with our experimental results[17,22,45,46].

Finally, our investigations allow for unambiguous interpretations because we intentionally investigated simple structures. Investigations of more complex systems are pursued now and will be published soon. In this paper, the detection of single atom trajectories by electron microscopy and the observed dynamic stabilization of characteristic displacements in graphene are reported, which could only be accomplished by applying deep sub-Ångstrom electron microscopy at 80kV using a microscope of extraordinary stability. Further, we point out that collective sample excitations probe the potential energy surface of a sample more complete than state-of-the-art calculations using single atom trajectories[64] and that the detection of extreme displacement values is of general interest in modeling rare but significant events[65]. Beyond these findings, the paper establishes a weak excitation approach for electron microscopy that is compatible with environmental[9] and time-resolved[12] transmission electron microscopy in broad beam mode.

Certainly, ionization or displacement of atoms proceeds constantly during the imaging process at any voltage and current and it will set an ultimate limit to the application of electron microscopy. Here we stress that contributions of phonon excitations are equally relevant and demonstrate that the existence of reversible system excitations matters greatly since it delays sample degradation to an unexplored end.

Acknowledgements

C. K. acknowledges fruitful discussions with P. Schwander and A. Ourmazd about their weak excitation approach, which they call “divide and conquer” and with S. Helveg about beam-sample interactions in electron microscopy and the relevance of these findings to chemical reaction pathways. Moreover he is grateful to N. Alem and Y. Li for the fabrication of electron transparent samples of graphene and STO, respectively. Electron Microscopy was performed at NCEM, which is supported by the Office of Science, Office of Basic Energy Sciences of the U.S. Department of Energy under Contract No. DE-AC02—05CH11231. The Dow Chemical Company supported P. Specht for the investigations of the rhodium catalysts. B. Barton and H. Calderon were supported by Helios SERC project to develop and apply low dose rate microscopy. HAC also acknowledges support through CONACYT (Grant 129207-FOINS75/2012). The work on collective excitations in carbon materials was performed for the Joint Center for Artificial Photosynthesis, a DOE Energy Innovation Hub, supported through the Office of Science of the U.S. Department of Energy under Award Number DE-SC0004993. Calculations were supported by the Office of Science, Office of Basic Energy Sciences, Materials Science and Engineering Division (MSE) of the U.S. Department of Energy under Contract No. DE-AC02-05CH11231. It uses resources of the National Energy Research

Scientific Computer Center (NERSC) and resources of the Oak Ridge Leadership Computing Facility located at the National Center for Computational Science, which is supported by the Office of Science, Office of Basic Energy Sciences of the U.S. Department of Energy under Contract No. DE-AC05—000R22775. Computer time was allocated by DOE's Innovative and Novel Computational Impact on Theory and Experiment (INCITE) Program.

REFERENCES

[1] W.U. Huynh, J.J. Dittmer, A.P. Alivisatos, Science 295, 2425-2427 (2002)

[2] N.S. Lewis, D.G. Nocera, Proc. of the National Academy of Sciences of the United States of America 103, 15729-15735 (2006)

[3] S.Y. Reece, J.A. Hamel, K. Sung, T.D. Jarvi, A.J. Esswein, J.J.H. Pijpers, D.G.Nocera, Science 334, 645-648 (2011)

[4] http://carboncycle2.lbl.gov/

[5]http://solarfuelshub.org/

[6]http://www.k-cap.or.kr/e_index.html

[7] S. Chenna, P.A. Crozier, ACS Catalysis 2, 2395-2402 (2012)

[8] J.F. Creemer, S. Helveg, G.H. Hoveling, S. Ullmann, A.M. Molenbroek, P.M. Sarro, H.W. Zandbergen, Ultramicroscopy 108, 993-998 (2008)

[9] H. Yoshida, Y. Kuwauchi, J.R. Jinschek, K. Sun, S. Tanaka, M. Kohyama, S. Shimada, M. Haruta, S. Takeda, Science 335, 317-319 (2012)

[10] J.R. Jinschek, S. Helveg, Micron 43, 1156-1168 (2012)

[11] N.D. Browning, M.A. Bonds, G.H. Campbell, J.E. Evans, T. LaGrange, K.L. Jungjohann, D.J. Masiel, J. McKeown, S. Mehraeen, B.W. Reed, M. Santala, Current Option in Solid State Science 16, 23-30 (2012)

[12] A.H. Zewail, Scientific American 303, 74-81 (2010)

[13] C. Kisielowski, B. Freitag, M. Bischoff, H. van Lin, S. Lazar, G. Knippels, et al., Microsc. Microanal. 14, 454-462 (2008)

[14] R. Erni, M.D. Rossell, C. Kisielowski, U. Dahmen, U.; Phys. Rev. Lett. 102, 096101 (2009)

[15] N. Alem, O.-V. Yazyev, C. Kisielowski, P. Denes, U. Dahmen, P. Hartel, M. Haider, S. Uhlemann, B. Jiang, S.G. Louie, A. Zettl, Phys. Rev. Lett. 106, 1261023 (2011)

[16] O.L. Krivanek, M. F. Chisholm, V. Nicolosi, T.J. Pennycook, G. J. Corbin, N. Dellby, M.F. Murfitt, S. S. Own, Z. S. Szilagyi, M. P. Oxley, S. T. Pantelides, S. J. Pennycook, Nature 464, 571-574 (2010)

[17] A.V. Martin, K. Ishizuka, C. Kisielowski, L.J. Allen, Phys. Rev. B 74, 172102 (2006)

[18] R.M. Wang, O. Dmitrieva, M. Farle, G. Dumpich, H.Q. Ye, H. Poppa, R. Kilaas, C. Kisielowski, Phys. Rev. Lett. 100, 017205 (2008)

[19] R.M. Glaeser, K. Downing, D. De Rosier, W. Chiu, J. Frank, Electron Crystallography of Biological Macromolecules, Oxford University Press, New York, New York, 2007, pp. 131–134

[20] R.F. Egerton, P. Li, M. Malac, Micron 35, 399–409 (2004)

[21] B.E. Bammes, J. Jakana, M.F. Schmid, W. Chiu, J. Struct. Biol. 169, 331–341 (2010)

[22] P. Specht, R.J. Gulotty, D. Barton, R. Cieslinski, S. Rozeveld, J.H. Kang, O.D. Dubon, C. Kisielowski, Chem. Cat. Chem. 3, 1034-1037 (2011)

[23] A. Rose, J. Opt. Soc. America 38, 196-208 (1948)

[24] J. Hemminger, chair, Basic Energy Advisory committee, Directing matter and energy: Five Challenges for science and imagination, http://science.energy.gov/bes/news-and-resources/reports/basic-research-needs/

[25] H.N. Chapman, P. Fromme, A. Barty, T.A. White, R.A. Kirian, A. Aquila, et al., Nature 470, 72-78 (2011)

[26] R. Fung, V. Shneerson, D.K. Saldin, A. Ourmazd, Nature Physics 5, 64-67 (2009)

[27] P. Schwander, R. Fung, G.N. Phillips, A. Ourmazd, New J. Phys. 12, 035007 (2010)

[28] A. Howie, Ultramicroscopy 98, 73–79 (2004)

[29] B. Barton, B. Jiang, C.Y. Song, P. Specht, H. Calderon, C. Kisielowski, Microsc. Microanal. 18, 982–994 (2012)

[30] S.M. Schramm, S.J. van der Molen, R.M. Tromp, Phys Rev. Lett. 109, 163901 (2012)

[31] Kisielowski, C.; Hetherington, C.J.D.; Wang, Y.C.; Kilaas, R.; O'Keefe, M.A.; Thust, A., Ultramicroscopy 2001, 89, 243-263

[32] P.C. Tiemeijer, M. Bischoff, B. Freitag, C. Kisielowski, Ultramicroscopy 114, 72-81 (2012)

[33] P.C. Tiemeijer, M. Bischoff, B. Freitag, C. Kisielowski, Ultramicroscopy 118, 35-43 (2012)

[34] X. Xu, S.P. Beckman, P. Specht, E.R. Weber, D.C. Chrzan, R.P. Erni, I. Arslan, N. Browning, A. Bleloch, C. Kisielowski, Phys. Rev. Lett. 95, 145501 (2005)

[35] M. Lentzen, Microsc. Microanal. 14, 16-26 (2008)

[36] O.W. Saxton, W. Baumeister, J. Microsc. 127, 127-138 (1982)

[37] http://www.totalresolution.com

[38] J.P. Perdew, K. Burke, M. Ernzerhof, Phys. Rev. Lett. 77, 3865-3868 (1996)

[39] G. Kresse, D. Jouber, Phys. Rev. B 59, 1758-1775 (1999)

[40] http:// www.vasp.at

[41] G. Henkelman, B.P. Uberuaga, H. Jonsson, Chem. Phys. 113, 9901-9904 (2000)

[42] A.G. Whittaker A.G.; Science 1978, 200, 763–764

[43] Ç. Ö. Girit, J.C. Meyer, R. Erni, M.D. Rossell, C. Kisielowski, L.Yang, C.-H. Park, M.F. Crommie, M.L. Cohen, S.G. Louie, A. Zettl, Science 323, 1705-1708 (2009)

[44] Alem, N.; Erni, R.; Kisielowski, C.; Rossell, M.D.; Gannett, W.; Zettl, A.; Phys. Rev. B 2009, 80, 155425

[45] C. Kisielowski, Q.M. Ramasse, L.P. Hansen, M. Brorson, A. Carlsson, A.M. Molenbroek, H. Topsoe, S. Helveg, Angewandte Chemie-Internat. edition 49, 2708-2710 (2010)

[46] D. Alloyeau, B. Freitag, S. Dag, L.-W. Wang, C. Kisielowski, Phys. Rev. B 80, 014114 (2009)

[47] E.J. Kirkland, Advanced computing in Electron Microscopy, Springer-Verlag New York, 2010

[48] L. Wang, Q. Ge, Chem. Phys. Lett. 366, 368–376 (2002)

[49] T. Abe, Y. Mizutani, N. Shinoda, M. Asano, T. Harada, M. Murakami, J. Phys. Chem. 57, 783-786 (1996)

[50] V.S. Steckline, Am. J. Phys. 51, 894-897 (1983)

[51] L. Wirtz, A. Rubio, Sol. State Comm. 131, 141-152 (2004)

[52] C. Jin, H. Lan, L. Peng, K. Suenaga, S. Iijima, Phys. Rev. Lett. 102, 205501 (2009)

[53] A. Chuvilin, J.C. Meyer, G. Algara-Siller, U. Kaiser, New J. Phys. 11, 083019 (2009)

[54] K.S. Pitzer, E. Clementi, J. Am. Chem. Soc. 81, 4477-4485 (1959)

[55] R.B. Heinemann, J. Kleiman, N.M. Salansky, Nature 306, 164-167 (1983)

[56] M.J. Rice, S.R. Phillpot, A.R. Bishop, D.K. Campbell, Phys. Rev. B 34, 4139–49 (1986)

[57] M.A. O'Keefe, Ultramicroscopy 47, 282-277 (1992)

[58] N. Jiang, J.H.C. Spence, Ultramicroscopy 113, 77–82 (2012)

[59] B. Schroeder, J. Geiger, Phys. Rev. Lett. 28, 301-303 (1972)

[60] L. Raimer, Transmission Electron Microscopy, Springer, Optical Series, New York 1993

[61] S. Schaefer, W. Liang, A.H. Zevail, New J. Phys. 13, 063030 (2011)

[62] H. Zheng, J.B. Rivest, T.A. Miller, B. Sadtler, A. Lindenberg, M.F. Toney, L.-W. Wang, C. Kisielowski, A.P. Alivisatos, Science 333, 206-209 (2011)

[63] B. Jouffrey, M. Karlik, Microscopy Microanalysis Microstructure 3, 243-357 (1992)

[64] F. Abild-Petterson, J.K. Norscov, J.R. Rostrup-Nielson, J. Sehested, S. Helveg, Phys. Rev. B 73, 115419 (2006)

[65] P. Joyce, D.R. Rokyta, C.J. Beisel, H.A. Or, Genetics 180, 1627-164 (2008)

See Supplemental Material Movie-Rh.avi and Movie-C.avi at [URL]

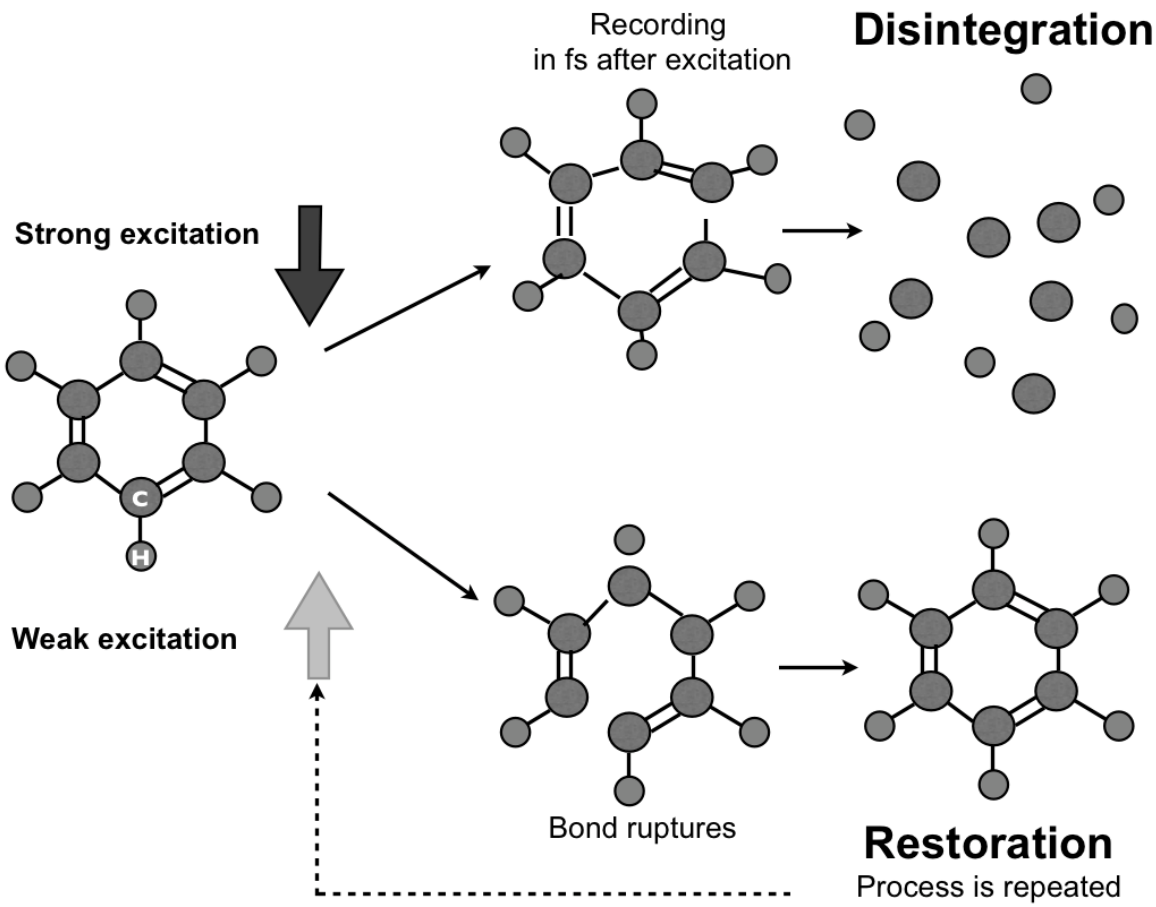

FIGURE 1: Schematic representation of a "strong excitation" (top) and a "weak excitation" (bottom) experiment. For simplicity a benzene ring is depicted but the schematics may also describe any atom cluster on an undefined substrate.

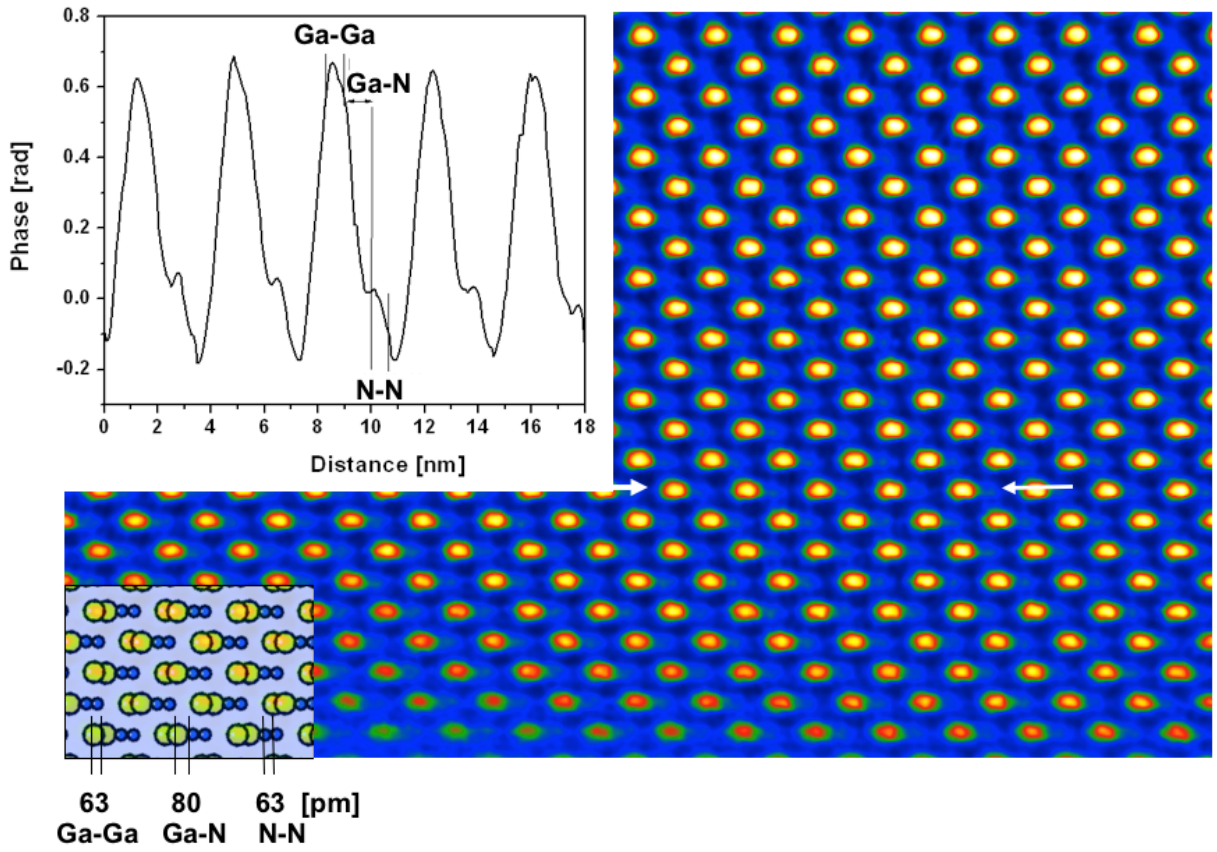

FIGURE 2: Phase image of a GaN [112] in-line hologram recorded at 80 kV. The contrast of the Ga and N columns differ largely because it scales with the atomic number $Z^{2/3}$. At the bottom of the image the crystal is 1-2 nm thick. A structure model and a line profile is inserted showing the 80 pm separation of Ga and N dumbbells and the 63 pm separation within each Ga or N dumbbell. The elliptical shape of the Ga contrast the lower half of the image is caused by the barely resolved Ga columns with a geometrical separation of 63 nm as shown in the extracted line profile.

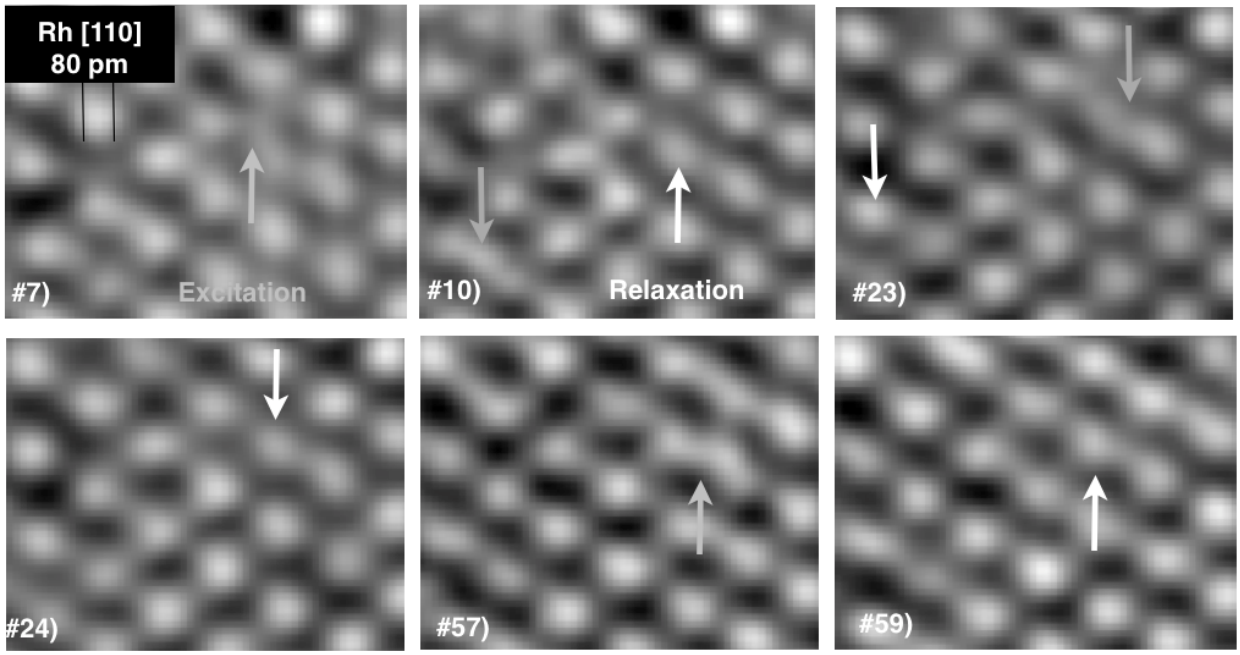

FIGURE 3: Six structural images from a time series of 60 images of a rhodium catalyst in [110] projection. Image acquisition numbers are listed. Dose rate: 6 10^5 e/nm^2/s. Gray arrows point to beam-induced atom displacements > 60 pm that relax in successive frames (white arrows). The image contrast greatly fluctuates (see supplementary movie-Rh).

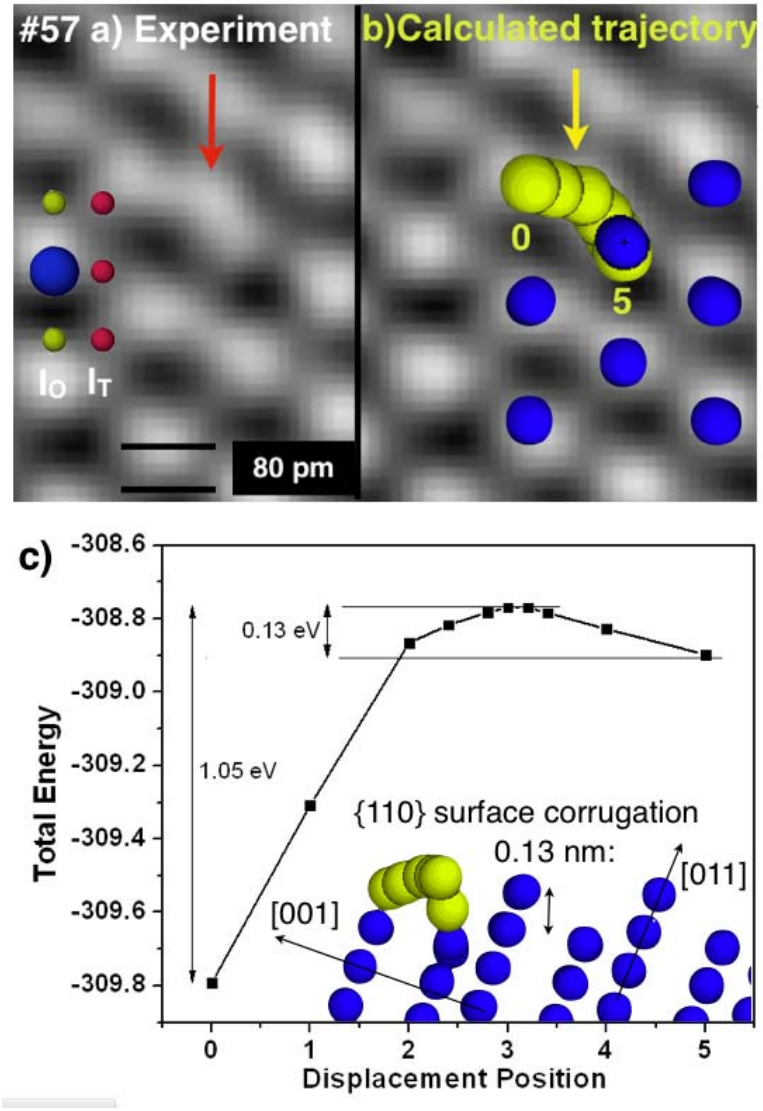

FIGURE 4: a) Temporary atom displacement in frame #57 marked by arrow. Selected sites are pointed out. Dark circles: Rh lattice sites. Small light and dark circles: octahedral and tetrahedral interstitial sites I_O and I_T. b) A calculated excitation / relaxation trajectory (0 - 5, bright circles) that matches the spatial distribution of the temporary image contrast in frame #57. c) Total energy calculations for the displacement. Inset: Projected view of the corrugated Rh [110] surface in slab geometry.

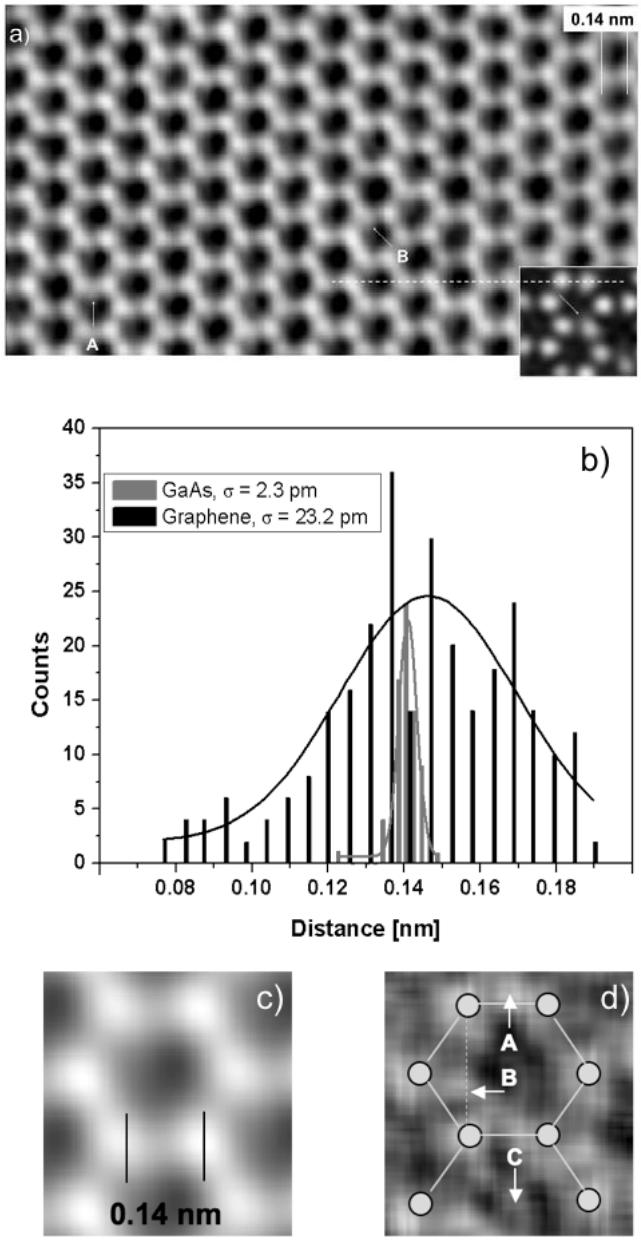

FIGURE 5: a) Phase image of graphene. Accumulated electron dose: 4 10^7 e/nm^2. The inset is an image simulation of contrast fluctuations that are caused by atom displacements from MD simulations at 0.75 T_m. b) Histogram of the C-C dumbbell distance in image a) and an equivalent measurements from GaAs[34]. c) Average motive in image a). d) The corresponding standard deviation amplifies reoccurring contrast in specific locations A, B and perhaps C in unexpected sites.

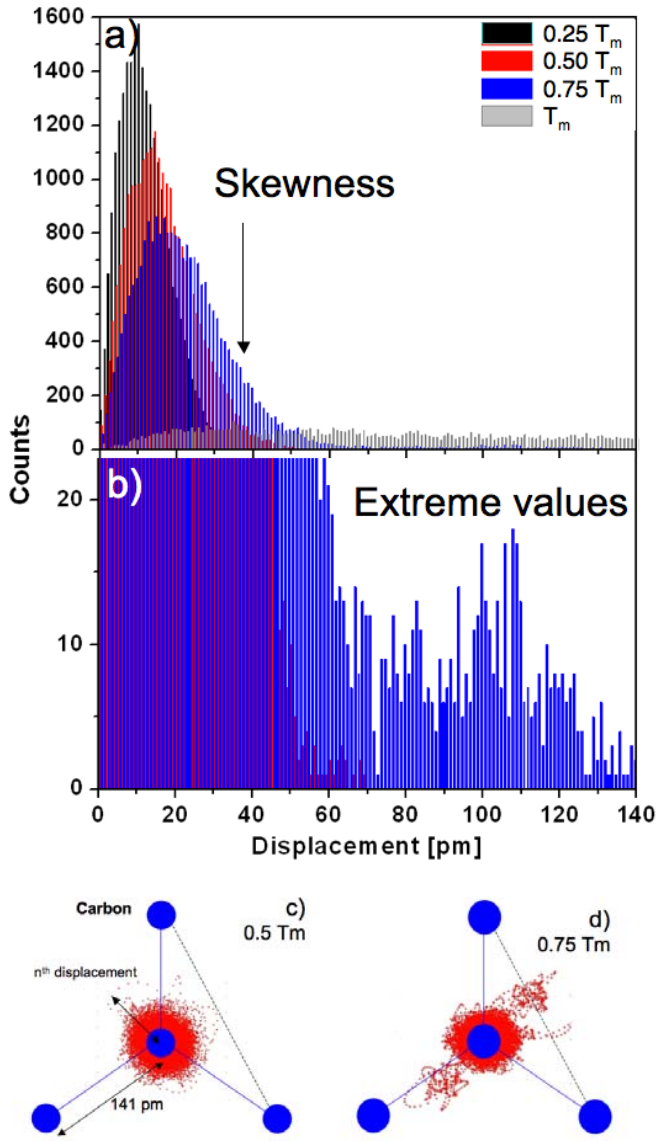

FIGURE 6: MD simulations at four different temperatures. a) Histogram of the projected atom displacements from their equilibrium position highlighting the skewness of the distributions. b) Magnified view emphasizing extreme displacement values > 30 pm that exceed reasonable Debye-Waller factors for 0.5 T_m and 0.75 T_m. c) Spatial distribution of 24000 carbon atom displacements for 0.5 T_m and d) for 0.75 T_m. The radius of the circles reflects the most common displacements (Debye-Waller factor).

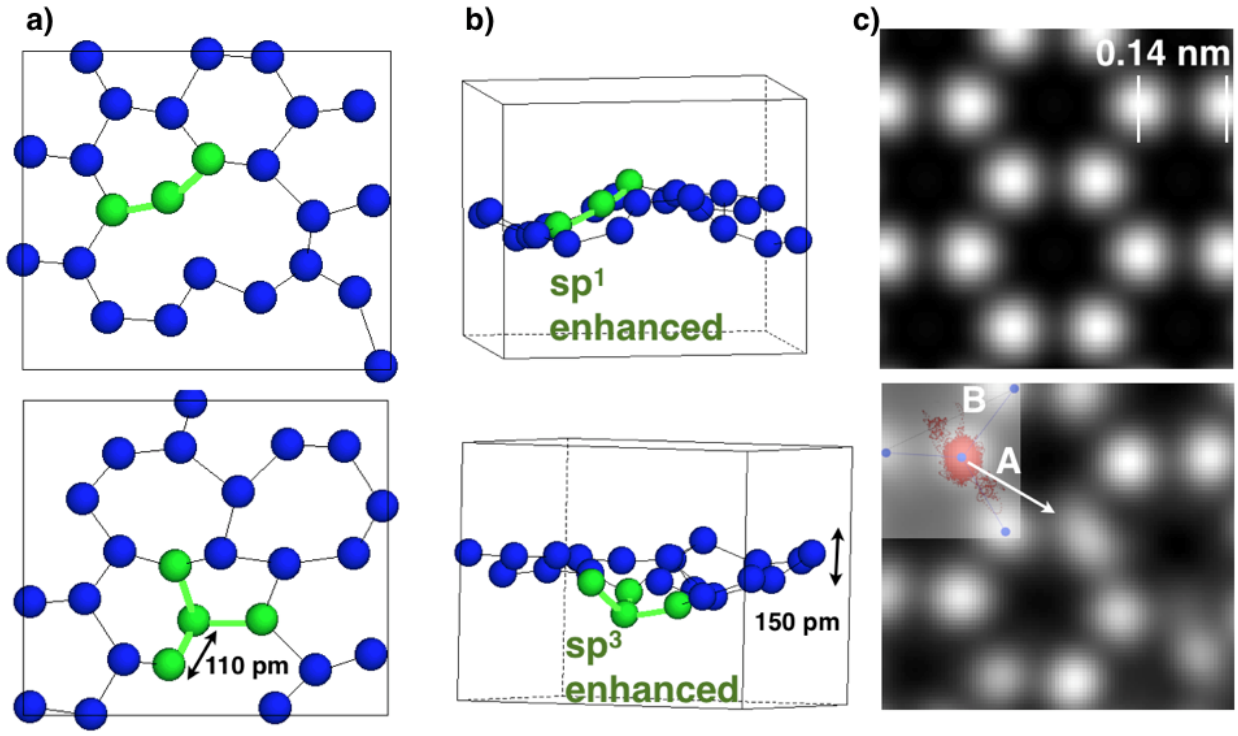

FIGURE 7: Two MD simulation snapshots at 0.75 T_m of graphene in top view (a) and side view (b). c) Lattice image by multislice simulations; top: static structure with B = 1Å^2. Bottom: B = 1Å^2 and using a 100 fs time average of the calculated MD configuration as an input. The inset is Fig. 6d.

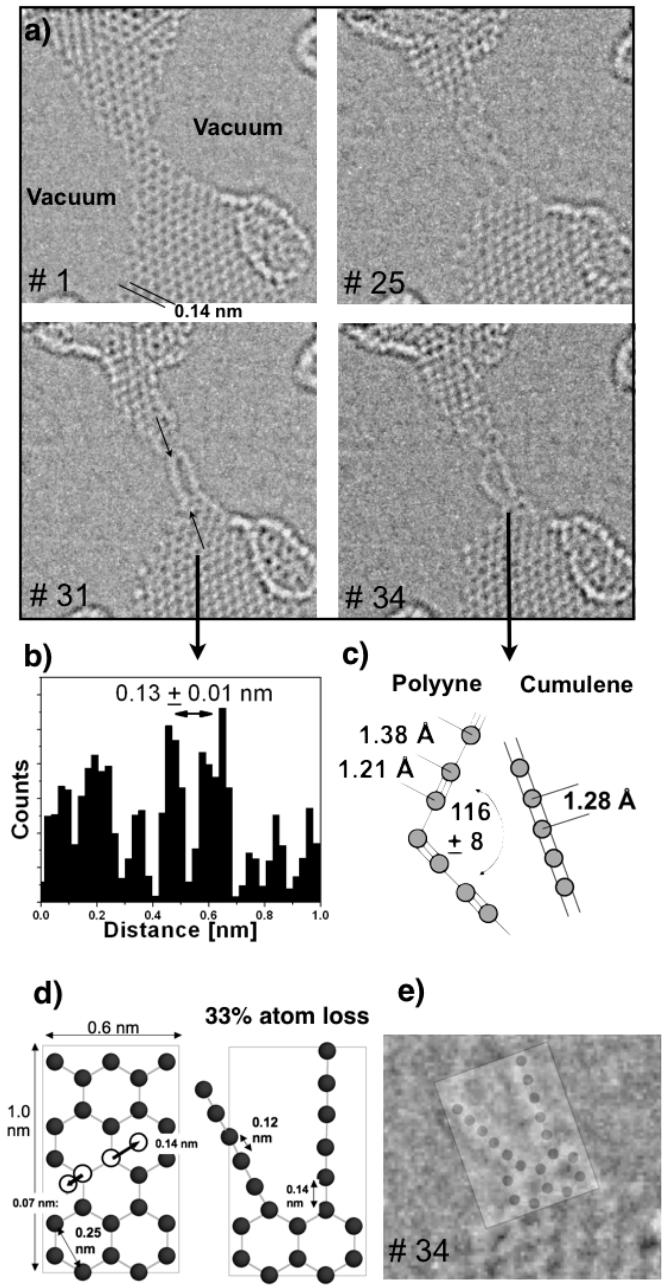

Figure 8: a) Time resolved measurement of a carbyne chain formation from a graphene bridge. Four frames of a time series of 40 images are shown. The time interval between successive images is 1.4s. b) Atomic resolution is obtained in frame #31. c) Theoretical bond distances and models of polyyene and cumulene are displayed. d) Geometrical transformation of graphene into carbyne as a result of atom displacements from lattice sites into positions B and C of Fig. 5d). e) Comparison of the model with the experiment in frame # 34.

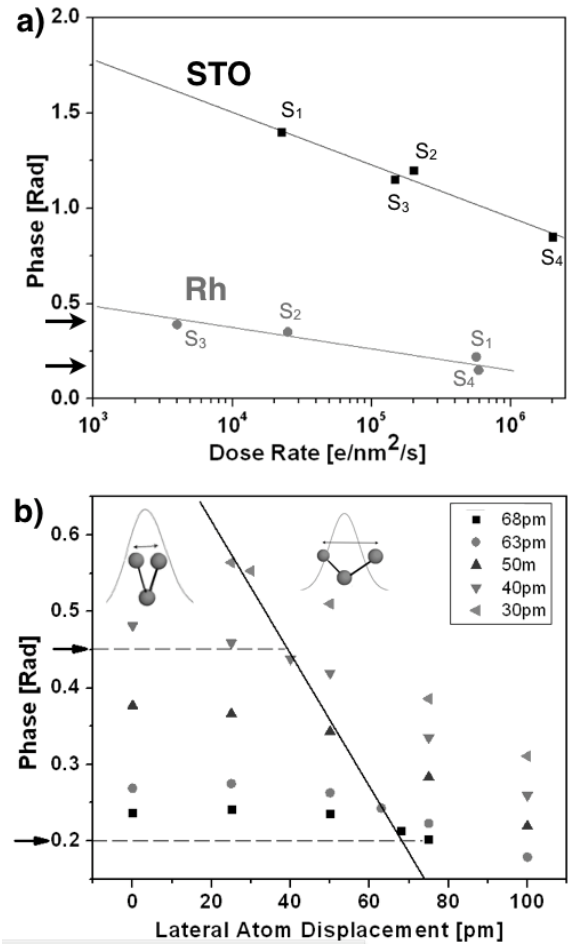

Figure 9: a) Measured logarithmic decrease of the image contrast with dose rates in phase images of reconstructed electron exit wave functions. Focus series from identical areas of the rhodium catalysts and a STO confirmation sample were reconstructed from 60 images in a series. S_i i = 1-4 labels their recording sequence. b) Contrast in simulated phase images from two rhodium atoms in an isolated column on lateral atom displacements of the top atom. Simulated phase images were reconstructed from simulated focus series of 10 images using the listed vibration amplitudes as an input to a Gaussian damping function. The solid line separates regions where the lateral displacements are either larger or smaller than the average vibration as symbolized by the inserted schematics. Broken horizontal lines and arrows frame an identical phase range in a) and b).

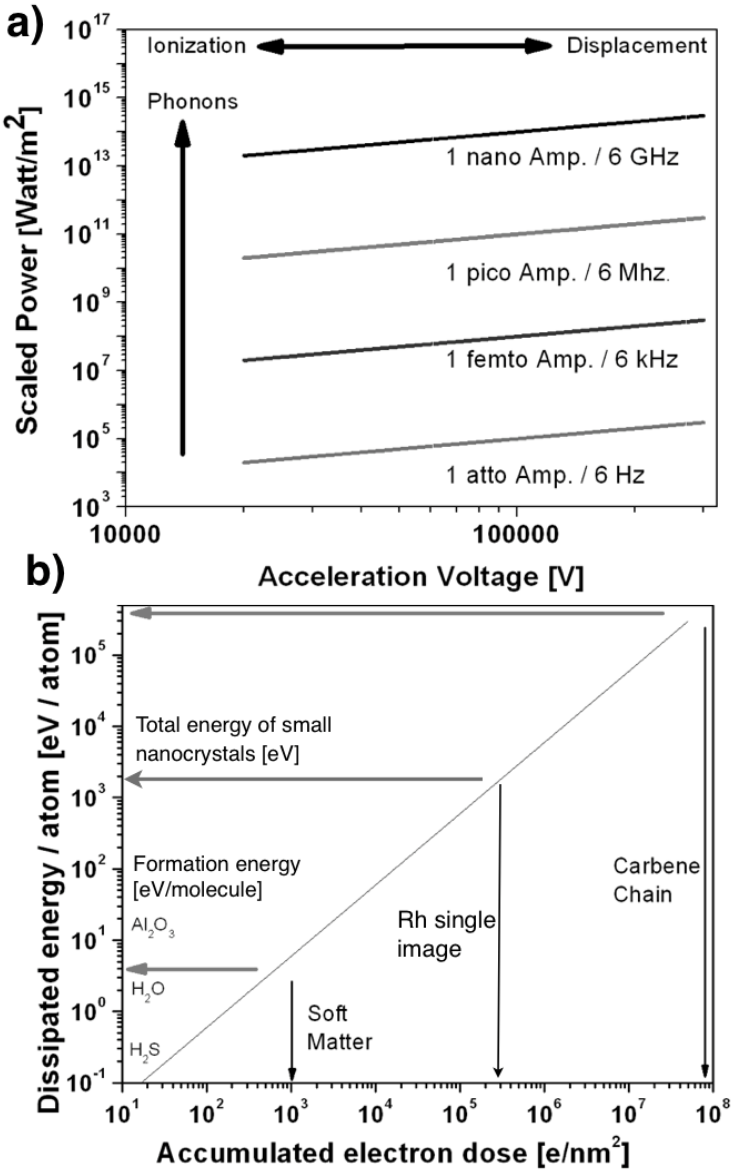

Figure 10: a) Available parameter space to perform dose rate dependent atomic resolution electron microscopy. Arrows point towards increasing beam-sample interactions as a result of specific interactions. b) Energy deposition in carbon materials. Characteristic, accumulated electron doses are marked and compared with formation energies of selected molecules or nanocrystals.

TABLES

Melting point temperature Tm	Maximum [pm] / Debye - Waller [Å²]	Displacements > 30 pm	Skewness
~ Tm	-	23925 / 99.7%	0.08
0.75 Tm	18 / 2.6	5620 / 23%	1.75
0.5 Tm	14 / 1.5	990 / 4%	0.81
0.25 Tm	11 / 0.96	147 / 0.6%	0.49

TABLE 1: Characteristic values of the projected bond length distributions in graphene that are shown in Figure 6 a).